

Spin density in YTiO₃: II. Momentum-space representation of electron spin density supported by position-space results

Z. Yan,¹ I. A. Kibalin,^{2,3} N. Claiser,³ S. Gueddida,¹ B. Gillon,² A. Gukasov,² A. B. Voufack,³ F. Morini,³ Y. Sakurai,⁴ M. Brancewicz,⁴ M. Itou,⁴ M. Itoh,⁴ N. Tsuji,⁴ M. Ito,⁵ M. Souhassou,³ C. Lecomte,³ P. Cortona,¹ and J.-M. Gillet^{1,*}

¹SPMS, UMR8580, CentraleSupélec, Université Paris-Saclay, Grande Voie des Vignes, Chatenay-Malabry Cedex 92295, France

²Laboratoire Léon Brillouin, CEA Centre National de la Recherche Scientifique, CE-Saclay, Gif-sur-Yvette 91191, France

³CRM2, Institut Jean Barriol, University of Lorraine, and UMR Centre National de la Recherche Scientifique 7036, Vandoeuvre-les-Nancy BP 70239, F54506, France

⁴Japan Synchrotron Radiation Research Institute, Mikaduki, Sayo, Hyogo 679-5198, Japan

⁵Faculty of Science and Technology, Gunma University, Kiryu, Gunma 376-8515, Japan

(Received 5 May 2017; published 21 August 2017)

Unpaired electrons in YTiO₃ ferromagnetic crystal (below 30 K) were studied by polarized neutron diffraction (PND) and incoherent x-ray magnetic Compton scattering (MCS). These experiments provide both position and momentum representations of the electrons at the origin of the magnetic behavior, mostly those in the t_{2g} state of Ti atoms. A two-dimensional reconstruction was conducted from experimental and theoretical directional magnetic Compton profiles to obtain the two-dimensional magnetic electron momentum density. A “superposition” method is proposed to examine the coherence between results for position and momentum spaces, respectively. This model-free approach allows a straightforward cross-checking of PND and MCS experiments. An “isolated Ti model” is proposed to emphasize the role played by O₁ in the ferromagnetic coupling between Ti and its neighboring atoms.

DOI: 10.1103/PhysRevB.96.054427

I. INTRODUCTION

Perovskite YTiO₃ (Fig. 1) is a ferromagnetic crystal at low temperature (below 30 K) [1]. The magnetic properties are widely accepted to result from a single d electron in a t_{2g} state localized on each Ti atom [2]. As this electron plays a crucial role in the control of the magnetic properties of YTiO₃, a precise determination of the electronic state is necessary. The electron probability density in position space, $\rho(\mathbf{r})$, can be determined from x-ray diffraction (XRD), and the electron-spin probability density in position space, $\rho_{\text{mag}}(\mathbf{r})$, can be determined from polarized neutron diffraction (PND) using models such as that proposed by Hansen and Coppens [3]. Combining these two techniques in the refinement of a unique model provides the spin resolved electron density using the spin-split pseudoatoms extension of the Hansen-Coppens model [4,5]. However, XRD and PND techniques have limited potential for observing the most diffuse electrons, which play an important role in many properties. As a complementary technique, incoherent x-ray inelastic scattering, in the large momentum and energy transfer limit (referred to as “Compton scattering”), can be employed to observe delocalized electrons. For a scattering vector pointing to the direction given by unit vector \mathbf{u} , the signal is related to the electron probability density in momentum space $n(\mathbf{p})$. To be more specific, the Compton scattering signal, for a scattering vector aligned with \mathbf{u} , is proportional to the so-called directional Compton profiles (DCPs) $J(\mathbf{u}, q)$:

$$J(\mathbf{u}, q) = \int n(\mathbf{p}) \delta(\mathbf{u} \cdot \mathbf{p} - q) d\mathbf{p}. \quad (1)$$

The DCP is thus the probability density for an electron of having a momentum q along direction \mathbf{u} , whatever the values

of the other two components. Expression (1) shows that the DCP is a projection of $n(\mathbf{p})$ on a particular vectorial line of momentum space. Therefore, two-dimensional (2D) [6–8] or three-dimensional [9–14] electron density in the momentum representation $n(\mathbf{p})$ can be reconstructed from a set of such projections.

Both $\rho(\mathbf{r})$ and $n(\mathbf{p})$ are thus electron-density descriptions in different representations. They can be connected through the one-electron reduced density matrix (1-RDM) [15] $\Gamma(\mathbf{x}, \mathbf{x}')$, which contains all the information at the one-electron level. If the spin variable is included, the 1-RDM is constructed from the N -electron wave function according to

$$\Gamma(\mathbf{x}, \mathbf{x}') = N \int \Psi^*(\mathbf{x}, \mathbf{x}_2, \dots, \mathbf{x}_N) \times \Psi(\mathbf{x}', \mathbf{x}_2, \dots, \mathbf{x}_N) d\mathbf{x}_2 \dots d\mathbf{x}_N \quad (2)$$

where \mathbf{x} represents the spin and position variables. In this paper, we concentrate on the spin properties and the magnetic 1-RDM can be obtained from spin resolved 1-RDMs:

$$\Gamma_{\text{mag}}(\mathbf{r}, \mathbf{r}') = \Gamma^{\uparrow}(\mathbf{r}, \mathbf{r}') - \Gamma^{\downarrow}(\mathbf{r}, \mathbf{r}') \quad (3)$$

where \uparrow and \downarrow refer to up- and down-spin states, respectively, and \mathbf{r} and \mathbf{r}' refer to the position variables. By definition, the spin density in position space $\rho_{\text{mag}}(\mathbf{r})$ is given by the diagonal elements ($\mathbf{r} = \mathbf{r}'$) of the magnetic 1-RDM:

$$\rho_{\text{mag}}(\mathbf{r}) = \Gamma_{\text{mag}}(\mathbf{r}, \mathbf{r}) \quad (4)$$

and, shifting to the momentum-space representation, similar quantities can be defined:

$$n_{\text{mag}}(\mathbf{p}) = \tilde{\Gamma}_{\text{mag}}(\mathbf{p}, \mathbf{p}), \quad (5)$$

which is the value for $\mathbf{p} = \mathbf{p}'$ of the 1-RDM matrix in momentum space:

$$\tilde{\Gamma}_{\text{mag}}(\mathbf{p}, \mathbf{p}') = \int \Gamma_{\text{mag}}(\mathbf{r}, \mathbf{r}') e^{i\mathbf{r} \cdot \mathbf{p}} e^{-i\mathbf{r}' \cdot \mathbf{p}'} d\mathbf{r} d\mathbf{r}' \quad (6)$$

*Corresponding author: jean-michel.gillet@centralesupelec.fr

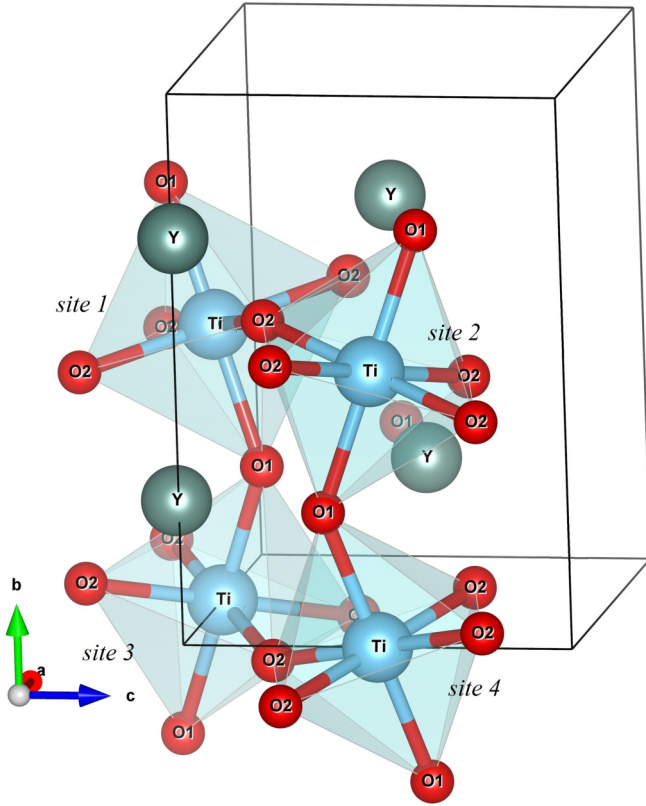


FIG. 1. Unit cell of perovskite YTiO_3 : space group $Pnma$, $a = 5.69 \text{ \AA}$, $b = 7.6094 \text{ \AA}$, $c = 5.335 \text{ \AA}$.

with \mathbf{p} representing the momentum of the electron and the directional magnetic Compton profile:

$$J_{\text{mag}}(\mathbf{u}, q) = \int n_{\text{mag}}(\mathbf{p}) \delta(\mathbf{u} \cdot \mathbf{p} - q) d\mathbf{p}. \quad (7)$$

In the present paper, where unpaired electrons are the focus of interest, PND and magnetic Compton scattering (MCS) techniques are probably the best suited tools for retrieving complementary information in position and momentum spaces.

The purpose of this paper is to shed light on how momentum-space quantities can be connected to the position-space densities presented in Ref. [16] and explain why delocalized unpaired electron density provides additional information. First, theoretical directional magnetic Compton profiles (DMCPs) are computed for comparison with experimental measurements. Second, both experimental and theoretical two-dimensional magnetic electron momentum densities (2D-MEMDs) are reconstructed from the DMCPs. Third, the “superposition” spin density is defined and shown to be coherent with the reconstructed magnetic momentum density. Finally, an “isolated Ti model” is used to better connect the position and momentum spaces. It emphasizes the ferromagnetic coupling along $\text{Ti-O}_1\text{-Ti}$ and shows that, while the interaction contribution between atoms is seldom considered in position space, the metal-oxygen coherent coupling can no longer be neglected for describing momentum-space properties.

II. DIRECTIONAL MAGNETIC COMPTON PROFILES

Experimental Compton profiles have been measured using the magnetic Compton scattering spectrometer on the high-energy inelastic-scattering beamline, BL08W, at Spring8 synchrotron radiation facility in Japan. Polarized x rays are emitted from an elliptical multipole wiggler and monochromatized to 175 keV before reaching the sample (single crystal with dimensions $1 \times 2 \times 3.5 \text{ mm}^3$). The energy of the scattered x rays at an angle of 178.5° is analyzed by a ten-segmented Ge solid-state detector. During the measurement, a $\pm 2.5\text{-T}$ external magnetic field was alternately applied along the scattering direction in order to reverse the sample magnetization in the 10–18-K temperature range. For each considered scattering direction, each DMCP was extracted as the difference between the two Compton profiles measured on the same sample magnetized in the opposite directions with a fixed photon helicity. The width of the elastic scattering peak provides an estimate of 0.4 a.u. for the momentum resolution of the magnetic spectrometer [17]. A total of 12 DMCPs were measured: along the principal axes a , b , and c ; $37(2)$, $55(2)$, and $72(2)^\circ$ from the axis a in the ab plane; and $22(2)$, $45(2)$, and $67(2)^\circ$ from the axes a and b in ac and bc planes, respectively. To serve as a reference, theoretical magnetic Compton profiles have been computed at the density functional theory (DFT) level, using the PBE0-1/3 [18] hybrid functional and atomic basis sets [19,20] as provided by the CRYSTAL14 package [21]. Generally, the purpose of DFT methods is not the computation of momentum-space properties [22,23] and such results have been shown to have recurrent flaws. Conversely, the Hartree-Fock (HF) method usually performs better [24,25] because it aims at optimizing a wave-function model. For YTiO_3 , HF computation turns out to suffer from severe convergence difficulties and it was found that a DFT approach converges much faster to a robust solution. Moreover, as shown below, the momentum-space properties computed from the Fourier transform of Kohn-Sham orbitals provide very satisfactory results [26].

As shown in Fig. 2, the theoretical and experimental DMCPs compare extremely well considering that less than 2% of electrons contribute to the inelastic magnetic signal. A more detailed analysis shows that for each direction of momentum space the theoretical distributions are systematically more localized than their experimental counterparts. Two reasons have previously been put forward: a possible functional effect on electron correlations as proposed by Huotari *et al.* [27] and thermal disorder. In the YTiO_3 case, we have tested a range of functionals (PBE0, PBE-1/3, PBESOL0, B3LYP, HISS, HSE06, BLYP) [18,28–34] and, except for BLYP, all of them result in very similar DMCPs. Given the low-temperature condition of the present experiment and that thermal smearing usually yields a contraction of momentum-space distributions [35], it is legitimate to also rule out this second source of broadening.

DMCPs (Fig. 2) reflect the unpaired electrons distribution in momentum (velocity) space. The ab plane exhibits the most isotropic results. Conversely the ac plane shows greater anisotropy: The bisecting direction is the lowest at low momenta, while it increases to reach a maximum around $q = 1$ (a.u.). This implies that, in position representation, the electrons are delocalized along the ac 45° direction, and more

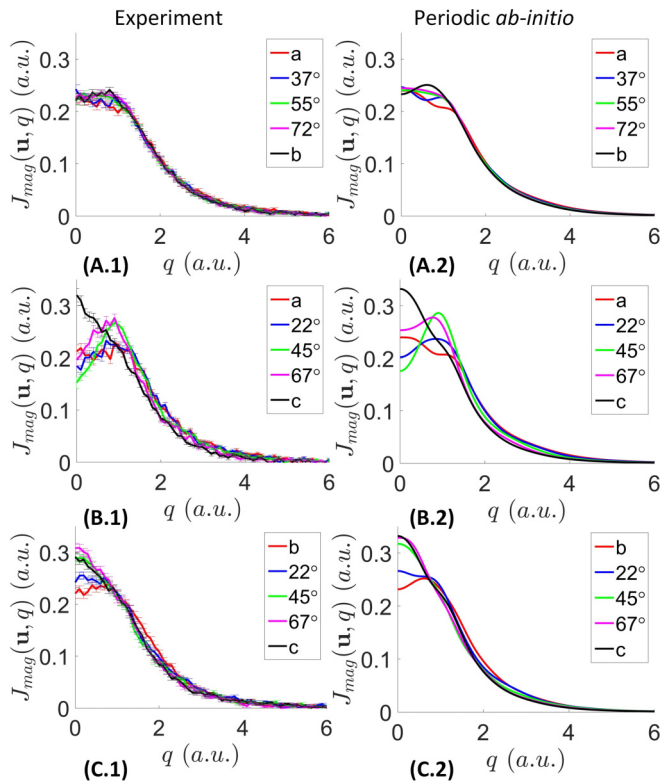


FIG. 2. Directional magnetic Compton profiles $J_{\text{mag}}(\mathbf{u}, q)$ for YTiO_3 for five nonequivalent directions \mathbf{u} in each plane. Each row corresponds to a set of DMCPs in a given plane: (a) ab plane, (b) ac plane, and (c) bc plane. The spectra are in atomic units and normalized to one electron. Left column: Experimental DMCP data points, given with their estimated error bars. Right column: Periodic *ab initio* DMCP, convoluted by a 0.4-a.u.-wide Gaussian resolution function.

localized along the \mathbf{a} or \mathbf{c} directions. The bc plane exhibits a significant difference between the \mathbf{b} and \mathbf{c} directions, with lower $J_{\text{mag}}(\mathbf{u}, q)$ values at low momenta in the \mathbf{b} direction.

III. TWO-DIMENSIONAL RECONSTRUCTION

DCPs or DMCPs can be used to reconstruct the momentum density $n(\mathbf{p})$ or the magnetic momentum density $n_{\text{mag}}(\mathbf{p})$, respectively. Reconstruction algorithms have been discussed by Hansen [36] and Dobrzynski and Holas [37]: The DCPs are used to compute directional reciprocal form factors or autocorrelation functions $B(\mathbf{u}, t)$ by Fourier transform:

$$B(\mathbf{u}, t) = \int J(\mathbf{u}, q) \exp(-iq \cdot t) dq \quad (8)$$

where \mathbf{u} is the unit vector collinear to the scattering vector and t refers to the relative position between two locations of the same particle along this direction. It is known as the “intracule position coordinate” along \mathbf{u} . From a limited set of directional $B(\mathbf{u}, t)$, corresponding to several nonequivalent scattering directions \mathbf{u} , an interpolated function $B(\mathbf{r})$ can be estimated. The momentum density can then be approximated

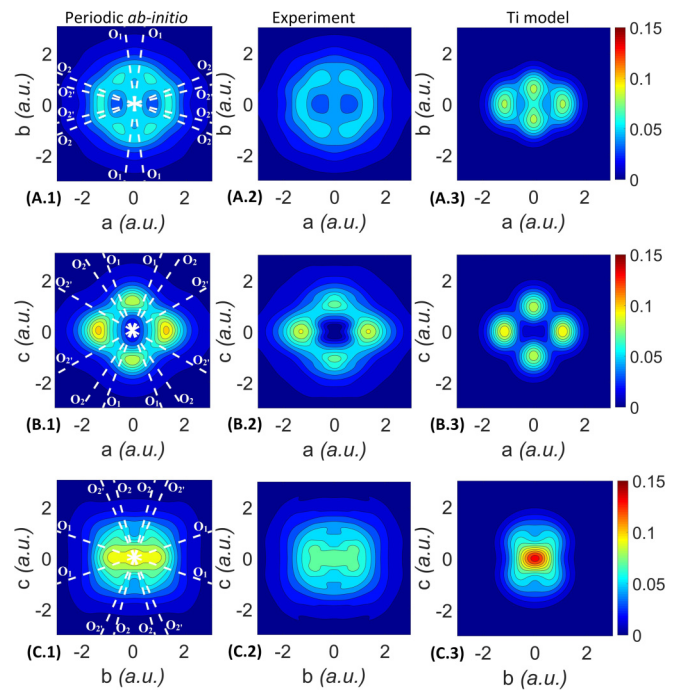


FIG. 3. Reconstructed spin density in momentum space (in a.u.), projected onto the three main crystallographic planes (2D-MEMD). Each row corresponds to a plane: (a) ab plane, (b) ac plane, and (c) bc plane. Left column: Periodic *ab initio* results using convoluted DMCPs, with white dashed lines indicating the projections of Ti-O directions in momentum space. Middle column: Experimental results. Right column: The same quantity obtained by the isolated Ti model (see Sec. V). Contours are at intervals of 0.01 a.u. Color bar scaling is from 0 to 0.15 a.u.

by inverse Fourier transform:

$$n(\mathbf{p}) = \frac{1}{(2\pi)^3} \int B(\mathbf{r}) \exp(i\mathbf{p} \cdot \mathbf{r}) d\mathbf{r}. \quad (9)$$

For this paper, the directional magnetic Compton profiles have been used to conduct 2D-MEMD reconstructions as projections of the magnetic momentum density in each of the above-mentioned planes. To avoid any interpretation bias in comparing theoretical and experimental 2D-MEMD, it was decided that both quantities should be recovered from their respective set of DMCPs by the same reconstruction procedure.

2D-MEMD anisotropies, defined as the difference between magnetic momentum density $n_{\text{mag}}(\mathbf{p})$ and the angular averaged isotropic density $n_{\text{mag}}^{\text{iso}}(p)$, can be calculated in each plane:

$$n_{\text{mag}}^{\text{aniso}}(\mathbf{p}) = n_{\text{mag}}(\mathbf{p}) - n_{\text{mag}}^{\text{iso}}(p). \quad (10)$$

As expected, these anisotropies are characteristic of the unpaired electron distribution upon the chemical bond formation and supplement the information available from diffraction data. If electrons on Ti sites are described from a pure crystal-field perspective, the spin momentum density can be seen to bear many features of the occupied atomic orbitals (in momentum representation) [8]. Results of Figs. 3 and 4 (left and middle columns) confirm the analysis of Fig. 2: The ab plane is the most isotropic with also the least informative

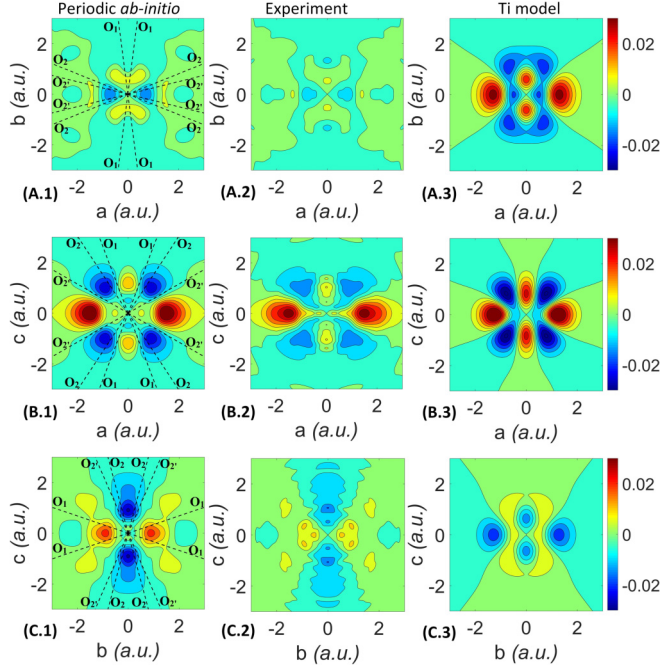


FIG. 4. Anisotropies of 2D-MEMD in each plane (in a.u.). Each row corresponds to a plane: (a) ab plane, (b) ac plane, and (c) bc plane. Left column: Periodic ab *initio* results using convoluted DMCPs, with white dashed lines indicating the projections of Ti-O directions in momentum space. Middle column: Experimental results. Right column: The same quantity obtained by the isolated Ti model (see also Sec. V). Contours are at intervals of 0.005 a.u. Color bar scaling is from -0.03 to 0.03 a.u.

features. In contrast, the ac plane displays a strong anisotropy, the projected momentum density is concentrated into well-resolved lobes near $(\pm 1.3, 0)$ and $(0, \pm 1.05)$ a.u., and the momentum density favors the a direction over c . Likewise, the bc plane exhibits a clear difference between b and c directions. From the crystal geometry (Fig. 1), the b direction approximately corresponds to the Ti-O₁-Ti interactions, while Ti-O₂-Ti lies parallel to the ac planes.

IV. ERROR ANALYSIS

An error propagation analysis is necessary to ensure the trustfulness of the experimental reconstruction and evaluate the significance of possible discrepancies with theoretical results. Experimental error bars on DMCPs are expected to impact the corresponding 2D-MEMD [38] and the following method has been used to simulate error propagation in the reconstruction process.

A Gaussian random distribution is assumed, the mean value and standard deviation of which are set to the experimental values $\{J_{\text{mag}}(\mathbf{u}, q_i)\}$ and associated error bars $\{\sigma[J_{\text{mag}}(\mathbf{u}, q_i)]\}$, respectively. The error propagation is thus estimated as follows (Fig. 5).

(1) Generate random DMCPs $\{J_{\text{mag}}^{\text{random}}(\mathbf{u}, q_i)\}$ following such a Gaussian distribution centered on the mean value $\{J_{\text{mag}}(\mathbf{u}, q_i)\}$.

(2) Renormalize to one electron each DMCP to obtain $\{J'_{\text{mag}}(\mathbf{u}, q_i)\}$ for each direction.

(3) Apply the reconstruction process to obtain a new 2D-MEMD $\{n_{\text{mag}}(\mathbf{p})\}$.

(4) Repeat N times steps 1 to 3, and perform a statistical analysis of the ensemble $\{n_{\text{mag}}(\mathbf{p})\}$ to evaluate a propagated error distribution $\sigma_{n(\mathbf{p})}$ for each plane.

For each direction, 1000 sets of random normalized DMCPs following a Gaussian distribution law were generated. As a result, 1000 reconstructions could be carried out. Such a statistical set is analyzed for estimating the influence of experimental uncertainty on the final 2D reconstruction of spin density in momentum space.

In order to assess the quality of the error propagation estimate, a simple test can be carried out using the theoretical DMCPs and the corresponding 2D-MEMD as a reference. For both quantities, theory-experiment agreement factors can be defined as

$$\chi^2_{J(\mathbf{u}, q)} = \frac{1}{N_{J(\mathbf{u}, q)}} \sum_{\mathbf{u}, q} \frac{[J_{\text{mag}}^{\text{theo}}(\mathbf{u}, q) - J_{\text{mag}}^{\text{exp}}(\mathbf{u}, q)]^2}{\sigma_{J(\mathbf{u}, q)}^2}, \quad (11a)$$

$$\chi^2_{n(\mathbf{p})} = \frac{1}{N_{n(\mathbf{p})}} \sum_{\mathbf{p}} \frac{[n_{\text{mag}}^{\text{theo}}(\mathbf{p}) - n_{\text{mag}}^{\text{exp}}(\mathbf{p})]^2}{\sigma_{n(\mathbf{p})}^2} \quad (11b)$$

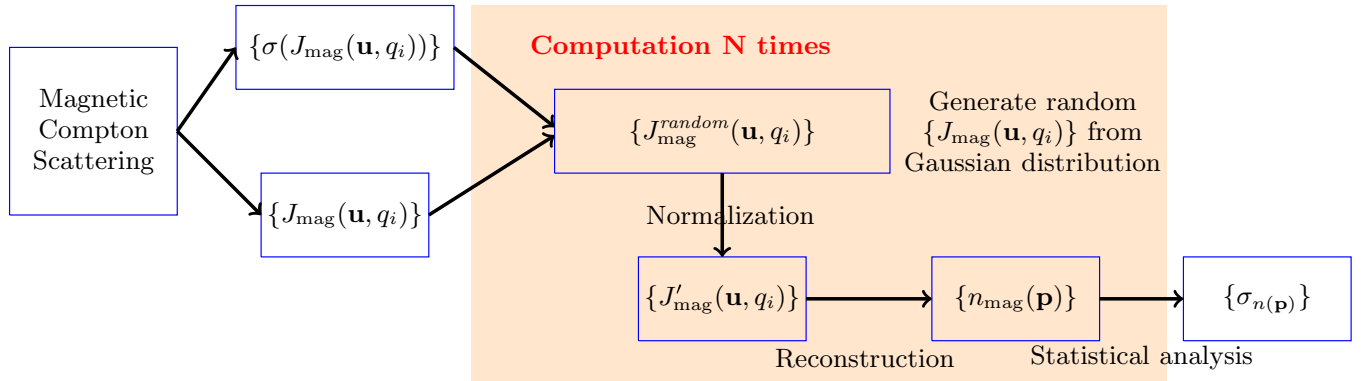


FIG. 5. Process of statistical error propagation analysis. $\{J_{\text{mag}}(\mathbf{u}, q_i)\}$ is the set of experimental values with the associated set of error bars $\{\sigma[J_{\text{mag}}(\mathbf{u}, q_i)]\}$. These values are used as the respective means and standard deviations of Gaussian distribution laws to randomly generate a large set of profiles (typically 1000) for each direction $\{J_{\text{mag}}^{\text{random}}(\mathbf{u}, q_i)\}$. Each of these profiles, by construction, falls within the experimental error bars. It thus becomes possible to conduct many reconstructions of 2D-MEMD, $\{n_{\text{mag}}(\mathbf{p})\}$. The statistical analysis of this set of reconstructions gives a fair estimate of the propagated error on the 2D-MEMD experimental reconstruction $\{\sigma_{n(\mathbf{p})}\}$.

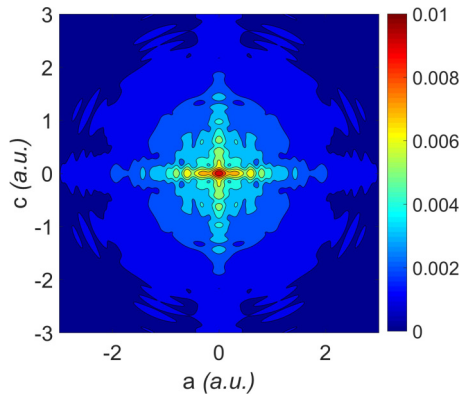


FIG. 6. Estimated propagation error map $\sigma_{n(\mathbf{p})}$ for reconstructed 2D-MEMD (in a.u.). The result is obtained by analysis of $N_{\text{times}} = 1000$ reconstructions in the ac plane with an adapted color bar scaling from 0 to 0.01 a.u. Contours are at intervals of 0.001 a.u.

where $N_{n(\mathbf{p})}$ and $N_{J(\mathbf{u}, \mathbf{q})}$ are the 2D-MEMD and DMCPs numbers of respective data points. These expressions indicate the extent of the discrepancy relative to the experimental standard deviations. While Eq. (11a), computed in the $p \in [-6, 6]$ -a.u. range, yields a value of 3.09, Eq. (11b) amounts to 3.02. These two values are very consistent and clearly indicate that the order of magnitude for reconstructed $\sigma_{n(\mathbf{p})}$ is trustworthy. Therefore, the reconstructed error reported in Fig. 6 shows very weak features compared with that of the experimental 2D-MEMD, and mostly concentrated in the $[-1, +1]$ -a.u. range.

Additionally, it can be noted that a $\chi^2 > 1$ value is an evidence that *ab initio* DMCPs or 2D-MEMD significantly deviate from experimental results. A refined model is thus necessary to make full use of experimental data, to identify the origin of discrepancies and to reconnect with position-space information.

V. COMPARISON BETWEEN TWO SPACE REPRESENTATIONS OF THE SPIN DENSITY

Electron densities in position and momentum spaces describe the electron behavior in a solid from different representations. However, it is difficult to analyze the chemical bond formation solely from a momentum perspective. In point of fact, most reported research make use of Compton scattering as a mere additional contribution to conduct a model refinement [39]. It was decided that, in this particular case, a joint analysis between PND and MCS deserves further exploration.

We propose here a method to reconsider the connection between position and momentum representations. Magnetic properties are expected to mostly result from a single d electron on the Ti site [2, 16]. However, a more thorough picture can be provided by a momentum-space study which emphasizes the behavior of the most delocalized unpaired electrons.

As a first approximation to the theoretical atomic spin population, a Mulliken partitioning analysis [40] yields the following results $\{\text{Y: } 0.043, \text{Ti: } 0.967, \text{O}_1: -0.006, \text{and } \text{O}_2: -0.002\}$. On the experimental result side, PND data [as well as those from magnetic x-ray diffraction (XMD)] presented in Ref. [16] have permitted us to reconstruct the spin-density

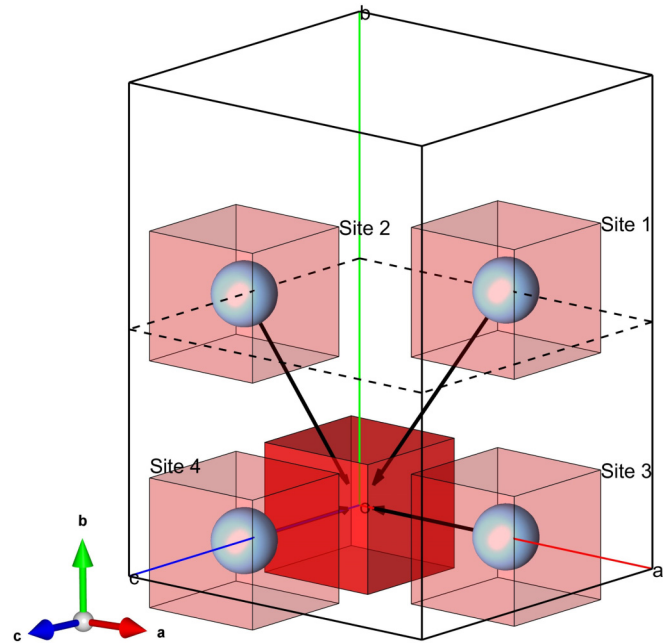


FIG. 7. Two steps to construct the superposition cube: (1) For a given unit cell, extract four cubes with 2-Å edges, centered on each Ti nucleus ($4b$ positions generated by space group symmetries [42]); (2) add up (and divide by 4) the respective spin-density distributions in the four cubes to obtain the superposition density cube.

distribution using the pseudoatomic wave-function model [41]. Parameters of the model include spin population for all atoms Y, Ti, and O. While the contribution of Ti clearly dominates with the 0.974 electron, experiments confirm the weak addition from O_1 , O_2 , and Y with an estimated value of 0.026.

To emphasize the coherence of experimental results for both position- and momentum-space representations, we propose a procedure. The respective contributions of the four Ti atoms (within the limits of a 2-Å cube) in the primitive cell are superimposed. The resulting averaged density is hereafter denoted as the “superposition representation” of the spin density, $\langle \rho_{\text{mag}}(\mathbf{r}) \rangle_{\text{Ti}}$, and computed as

$$\langle \rho_{\text{mag}}(\mathbf{r}) \rangle_{\text{Ti}} = \frac{1}{4} \sum_{n=1}^4 \rho_{\text{mag}}(\mathbf{r} + \mathbf{R}_n) \quad (12)$$

where \mathbf{r} is in the 2-Å cube, with $-1 \leq \{x, y, z\} \leq 1$ Å, and \mathbf{R}_n are the Ti nucleus positions at different sites (as shown in Fig. 7). The two-dimensional projections of the superposition spin density for the three planes perpendicular to the three crystallographic axes, respectively, are computed and compared with 2D-MEMD results in Fig. 8.

For each plane, the *ab initio* projected superposition spin density is slightly larger than its experimental counterpart. As previously mentioned, this can be attributed to the larger theoretical unpaired population on the Ti sites. A comparison of Figs. 3 and 8 highlights the striking similarity of projected superposition spin density with 2D-MEMDs for all planes. This method thus provides a possible means of checking the coherence between PND and MCS experiments. Moreover, this is visual confirmation that observing d electron density in momentum space (using Compton scattering data) is possible

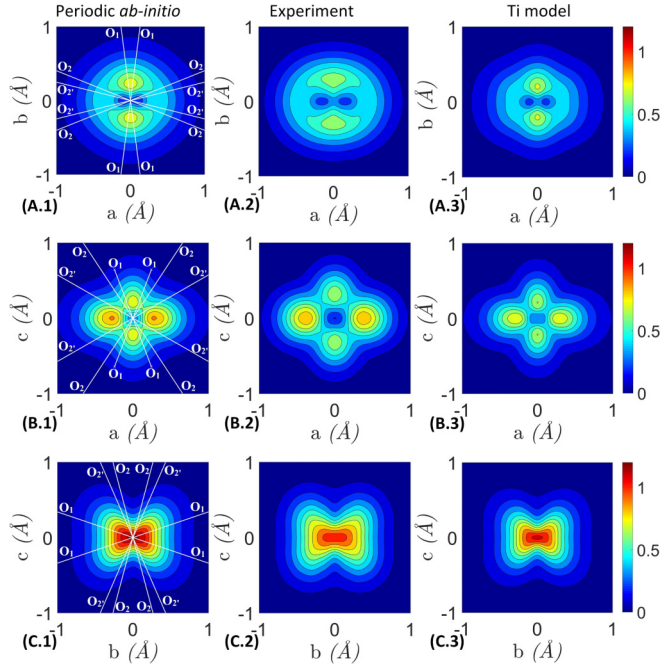


FIG. 8. Projections of the superposition spin density (in $\mu_B \cdot \text{\AA}^{-2}$) onto the three main crystallographic planes. Each row corresponds to a plane: (a) ab plane, (b) ac plane, and (c) bc plane. Left column: Periodic *ab initio* results, with white solid lines indicating the projections of oxygen positions in superposition space. Middle column: Experimental data. Right column: Single Ti orbital model. Contours are at intervals of $0.1 \mu_B \cdot \text{\AA}^{-2}$. Color bar scaling is from 0 to $1.2 \mu_B \cdot \text{\AA}^{-2}$.

in much the same way as it is (more commonly) done in position space. To provide a qualified explanation of this observation, an isolated Ti model can be used. It is first considered that the dominant contribution to the spin density comes from an unpaired electron on a Ti $3d$ -type orbital. Following a combination of symmetries suggested by Akimitsu *et al.* [43], we use the following expression for the local wave function:

$$|\psi\rangle = \sqrt{0.61}|yz\rangle + \sqrt{0.39}|xz\rangle \quad (13)$$

where the coefficients have been determined by the pseudoatomic wave-function refinement on PND data presented in Ref. [16]. Such a d orbital population anisotropy is also in excellent agreement with our recent electron-density modeling based on high-resolution x-ray-diffraction data [44]. A noticeable difference with the construction brought forward by Akimitsu *et al.* [43] is that the local y and z axes are reversed for site 1 and 2 with fractional coordinates: (0.5, 0.5, 0) and (0, 0.5, 0.5), respectively. The four Ti atoms are identical by symmetries ($4b$ positions in $Pnma$) [42], but cannot be superimposed by translations only. The local z direction is defined by the Ti-O₂ bond, while the local x and y directions are set approximately along the Ti-O₁ and the Ti-O₂ bonds, respectively.

In this isolated Ti model, the Ti atomic radial function for $|yz\rangle$ and $|xz\rangle$ is that given by Clementi and Roetti [45]. The model superposition density using expression (13) for each Ti contribution can then be computed as defined in Eq. (12). Similarly, the total spin density in momentum space results from a mere addition of the Ti sites' contributions. The

projections of the superposition density and the momentum density obtained by this isolated Ti model will be used for comparison with theoretical and experimental superposition spin density and 2D-MEMDs.

Figures 8 and 3 (right column) confirm the strong geometrical similarities between the superposition and momentum distributions. More importantly, a comparison of this result with the two other columns supports the dominant belief that a pseudoatomic model is often enough to qualitatively account for observations in position space. However, from Fig. 3, it is essential to note that the single Ti model is not fully adapted to reproduce momentum-space properties. While the model's 2D-MEMD (Fig. 3) and its anisotropy (Fig. 4) exhibit features which are quite comparable in the ac plane to those found from experiment (or *ab initio* results), this is no longer true for the momentum-space spin density projected onto the ab or bc planes. Obviously, the isolated Ti model is dominantly affected by discrepancies along the b direction for which the lack of coupling with the O₁ ($4c$ position) atom appears to have the strongest impact. It can thus be reasonably claimed that momentum-space properties, which are known to be more sensitive to delocalized electrons, support the role played for the unpaired electron by the coupling along the Ti-O₁-Ti chemical bond (close to the b direction). Therefore it qualifies this bond as a possible ferromagnetic pathway in YTiO₃.

In order to further validate such a mechanism, it becomes necessary to go beyond the single Ti picture for elaborating a local wave function. The joint use of PND, XMD, and DMCP data will thus be essential to refine a more sophisticated model accounting for the role played by unpaired electrons in the coupling between the metal and its oxygen atomic neighbors.

VI. CONCLUSION

With the aim of facilitating a possible comparison of information obtained from polarized neutron diffraction and magnetic Compton scattering experimental data, a construction called "superposition density" has been introduced. It is simply the accumulation of electron-spin densities from different atomic contributions translated to the same site. It can be projected onto any given plane. The pertinence of this construction is supported by periodic *ab initio* calculations at the DFT level. Geometrical similarities with 2D-MEMD are striking and confirm the coherence of experimental results but additional conclusions can be drawn. An estimate of the experimental uncertainties propagation through the 2D-MEMD reconstruction process shows that all observed experimental features, including those emphasized by momentum-space anisotropies, bear a significant physical meaning. In particular, the similarity of 2D-MEMD with superposition spin density clearly confirms that it provides a momentum-space representation of unpaired electron occupation in atomic spin orbitals. This is another demonstration of the results obtained by Sakurai *et al.* [8]. On the one hand, an isolated Ti model, using an optimized linear combination of Slater orbitals on Ti only, fairly reproduces the superposition spin density for all planes and reproduces rather well the 2D-MEMD in the ac plane. On the other hand, the strong sensitivity of momentum-space observables to delocalized electrons introduces significant

discrepancies in planes involving the Ti-O₁-Ti chemical bond direction. This very direction is thus identified as playing a major role in the spin delocalization and possibly the ferromagnetic coupling of metallic sites.

It can be concluded that a clearer understanding of the ferromagnetic mechanism pathway can be gained from a further detailed orbital model, involving both the Ti atom and its neighbors O₁. A more elaborate model, which thus involves the one-particle spin-density matrix, should be refined jointly from PND, XRD, XMD, and MCS data and is currently under development. It is expected that such a refinement should bring a more robust and deeper description of the subtle mechanisms at work in ferromagnetic compounds.

ACKNOWLEDGMENTS

Financial support from The French National Research Agency (ANR) (Multi-Techniques Modeling of Electron Densities (MTMED) project) and CNRS is gratefully acknowledged. The authors thank Y. Taguchi (Institute of Physical and Chemical Research (RIKEN)) for providing the samples. The magnetic Compton scattering experiments were performed with the approval of Japan Synchrotron Radiation Research Institute (JASRI) (Proposal No. 2014B1231). Z.Y. thanks China Scholarship Council (CSC) for Ph.D. scholarship support. A.B.V. thanks the Ministry of High Education and Scientific Research.

-
- [1] A. C. Komarek, H. Roth, M. Cwik, W.-D. Stein, J. Baier, M. Kriener, F. Bourée, T. Lorenz, and M. Braden, *Phys. Rev. B* **75**, 224402 (2007).
- [2] J. Hester, K. Tomimoto, H. Noma, F. Okamura, and J. Akimitsu, *Acta Crystallogr. Sect. B* **53**, 739 (1997).
- [3] N. K. Hansen and P. Coppens, *Acta Crystallogr. Sect. A* **34**, 909 (1978).
- [4] M. Deutsch, N. Claiser, S. Pillet, Y. Chumakov, P. Becker, J.-M. Gillet, B. Gillon, C. Lecomte, and M. Souhassou, *Acta Crystallogr. Sect. A* **68**, 675 (2012).
- [5] M. Deutsch, B. Gillon, N. Claiser, J.-M. Gillet, C. Lecomte, and M. Souhassou, *IUCr J* **1**, 194 (2014).
- [6] N. Hiraoka, T. Buslaps, V. Honkimäki, H. Minami, and H. Uwe, *Phys. Rev. B* **71**, 205106 (2005).
- [7] A. Koizumi, T. Nagao, N. Sakai, K. Hirota, and Y. Murakami, *Phys. Rev. B* **74**, 012408 (2006).
- [8] Y. Sakurai, M. Itou, B. Barbiellini, P. E. Mijnders, R. S. Markiewicz, S. Kaprzyk, J.-M. Gillet, S. Wakimoto, M. Fujita, S. Basak, Y. J. Wang, W. Al-Sawai, H. Lin, A. Bansil, and K. Yamada, *Science* **332**, 698 (2011).
- [9] N. K. Hansen, P. Pattison, and J. R. Schneider, *Z. Phys. B* **66**, 305 (1987).
- [10] Y. Tanaka, N. Sakai, Y. Kubo, and H. Kawata, *Phys. Rev. Lett.* **70**, 1537 (1993).
- [11] W. Schulke, G. Stutz, F. Wohler, and A. Kaprolat, *Phys. Rev. B* **54**, 14381 (1996).
- [12] J.-M. Gillet, C. Fluteaux, and P. J. Becker, *Phys. Rev. B* **60**, 2345 (1999).
- [13] Y. Tanaka, Y. Sakurai, A. T. Stewart, N. Shiotani, P. E. Mijnders, S. Kaprzyk, and A. Bansil, *Phys. Rev. B* **63**, 045120 (2001).
- [14] T. Nagao, Y. Kubo, A. Koizumi, H. Kobayashi, M. Itou, and N. Sakai, *J. Phys.: Condens. Mat.* **20**, 055201 (2008).
- [15] P.-O. Löwdin, *Phys. Rev.* **97**, 1474 (1955).
- [16] I. A. Kibalin, Z. Yan, A. B. Voufack, S. Gueddida, B. Gillon, A. Gukasov, F. Porcher, A. M. Bataille, F. Morini, N. Claiser, M. Souhassou, C. Lecomte, J.-M. Gillet, M. Ito, K. Suzuki, H. Sakurai, Y. Sakurai, C. M. Hoffmann, and X. P. Wang, *Phys. Rev. B* **96**, 054426 (2017).
- [17] More detailed information is available from http://www.spring8.or.jp/wkg/BL08W/instrument/lang-en/INS-000000358/instrument_summary_view.
- [18] C. A. Guido, E. Brémond, C. Adamo, and P. Cortona, *J. Chem. Phys.* **138**, 021104 (2013).
- [19] A. Buljan, P. Alemany, and E. Ruiz, *J. Phys. Chem. B* **103**, 8060 (1999).
- [20] A. Erba, K. E. El-Kelany, M. Ferrero, I. Baraille, and M. Rérat, *Phys. Rev. B* **88**, 035102 (2013).
- [21] C. Pisani, *Quantum-Mechanical Ab-Initio Calculation of the Properties of Crystalline Materials* (Springer, New York, 2012), Vol. 67.
- [22] L. Lam and P. Platzman, *Phys. Rev. B* **9**, 5122 (1974).
- [23] R. K. Pathak, A. Kshirsagar, R. Hoffmeyer, and A. J. Thakkar, *Phys. Rev. A* **48**, 2946 (1993).
- [24] J. R. Hart and A. J. Thakkar, *Int. J. Quantum. Chem.* **102**, 673 (2005).
- [25] S. Ragot, *J. Chem. Phys.* **125**, 014106 (2006).
- [26] A. Erba, C. Pisani, S. Casassa, L. Maschio, M. Schütz, and D. Usvyat, *Phys. Rev. B* **81**, 165108 (2010).
- [27] S. Huotari, K. Hämäläinen, S. Manninen, S. Kaprzyk, A. Bansil, W. Caliebe, T. Buslaps, V. Honkimäki, and P. Suortti, *Phys. Rev. B* **62**, 7956 (2000).
- [28] C. Adamo and V. Barone, *J. Chem. Phys.* **110**, 6158 (1999).
- [29] A. D. Becke, *J. Phys. A* **38**, 3098 (1988).
- [30] T. M. Henderson, A. F. Izmaylov, G. E. Scuseria, and A. Savin, *J. Chem. Phys.* **127**, 221103 (2007).
- [31] T. Henderson, A. Izmaylov, G. Scuseria, and A. Savin, in APS Meeting Abstracts, 2008 (unpublished), p. 13004.
- [32] A. V. Krukau, G. E. Scuseria, J. P. Perdew, and A. Savin, *J. Chem. Phys.* **129**, 124103 (2008).
- [33] C. T. Lee, W. T. Yang, and R. G. Parr, *Phys. Rev. B* **37**, 785 (1988).
- [34] J. P. Perdew, K. Burke, and M. Ernzerhof, *Phys. Rev. Lett.* **77**, 3865 (1996).
- [35] C. Sternemann, G. Doring, C. Wittkop, W. Schülke, A. Shukla, T. Buslaps, and P. Suortti, *J. Phys. Chem. Solids* **61**, 379 (2000).
- [36] N. K. Hansen, The Reconstruction of Momentum Density, in *X-Ray Compton Scattering*, edited by M. Cooper (Oxford University, New York, 2004).
- [37] L. Dobrzynski and A. Holas, *Nucl. Instrum. Methods Phys. Res. Sect. A* **383**, 589 (1996).
- [38] R. J. Barlow, *Statistics: A Guide to the Use of Statistical Methods in the Physical Sciences* (Wiley, New York, 1989), Vol. 29.
- [39] J.-M. Gillet, P. J. Becker, and P. Cortona, *Phys. Rev. B* **63**, 235115 (2001).
- [40] R. S. Mulliken, *J. Chem. Phys.* **23**, 1833 (1955).

- [41] B. Gillon and P. Becker, in *Modern Charge Density Analysis*, edited by C. Gatti and P. Macchi (Springer, Dordrecht, 2012).
- [42] M. I. Aroyo, *International Tables for Crystallography Volume A: Space-group Symmetry* (2016), Chap. 2.3, pp. 193–687.
- [43] J. Akimitsu, H. Ichikawa, N. Eguchi, T. Miyano, M. Nishi, and K. Kakurai, *J. Phys. Soc. Jpn.* **70**, 3475 (2001).
- [44] A. B. Voufack *et al.*, 2017 (private communication).
- [45] E. Clementi and C. Roetti, *At. Data Nucl. Data Tables* **14**, 177 (1974).